Electronic structure of fluorite-type compounds and mixed crystals

J. Kudrnovský*
Max-Planck-Institut für Festkörperforschung, Heisenbergstrasse 1, D-7000 Stuttgart 80, Germany

N. E. Christensen
Max-Planck-Institut für Festkörperforschung, Heisenbergstrasse 1, D-7000 Stuttgart 80, Germany
and Institute of Physics, Aarhus University, DK-8000 Aarhus C, Denmark

J. Mašek
Institute of Physics, Czechoslovak Academy of Sciences, Na Slovance 2, 180 40 Praha, Czechoslovakia
(Received 3 December 1990)

The electronic structures of fluorite-type crystals CaF_2, SrF_2, CdF_2, and PbF_2 are studied by means of the linear-muffin-tin-orbitals (LMTO) method. The tight-binding version of the LMTO and its coherent-potential-approximation (CPA) generalization is used to study the electronic states in $(Ca,Cd)F_2$, $(Pb,Sr)F_2$, and $(Ca,Sr)F_2$ mixed crystals. In the case of $(Cd,Pb)F_2$, we investigate the effects due to the large lattice-constant mismatch by introducing two extreme models of bond-length variations in the mixed crystals: (i) Mixed-crystal bond lengths preserve their values from pure crystals, and (ii) all bond lengths are varied linearly with the alloy composition between the pure crystal values. A comparison of the results with the photoemission data supports the former model, which is used also for other systems. As a side issue, we discuss the accuracy of the supercell approach to the electronic structure of random alloys by comparing LMTO supercell and LMTO-CPA calculations using the same set of potential parameters.

I. INTRODUCTION

The fluorite crystal structure ($C1$) is common to many interesting materials. Among them the compounds of fluorine with divalent metals, e.g., CaF_2, CdF_2, and PbF_2, constitute a family of fluorite-type crystals.[1] These are wide-gap insulators, which have been extensively studied experimentally in the past for their intrinsic optical properties.[2] More recently, new attention has been paid to the fluorite-type compounds and derived mixed crystals in connection with their superionic conductivity.[3]

The fluorite-type crystals are ionic with very similar bonding relations, irrespective of the fact that the cations belong to several groups of the Periodic Table and the underlying electronic structures may be largely different, as indicated by optical measurements.[4] The strongly electronegative fluorine captures two electrons from the cationic valence shell. The cations are then, for all fluorite-type compounds, characterized by an effectively compact electronic configuration. This is clear in the case of cations belonging to the group IIa of the Periodic Table (Ca,Sr,Ba,Ra), which have a closed-shell configuration in the fluorite-type crystals. In the case of the group IIb (Cd,Hg), there is a closed d^{10} configuration forming the soft core in the electronic spectrum. Finally, the valence shell of the group-IV cations, Sn^{2+} and Pb^{2+}, can be characterized as an inert-pair s^2 configuration. Due to these features of the bonding relations in the fluorite-type crystals, the cations can easily be replaced by another divalent metal ion. The substituents are either isoelectronic (e.g., CaF_2:Sr,Ba or PbF_2:Sn) or nonisoelectronic, but still isovalent, if the electronic configuration of the impurity valence shell differs from the one of the host cation. These are the physically most interesting cases, such as CdF_2:Ca,Pb or even CdF_2:Mn.[5] The isovalent substitution is possible up to high impurity concentrations. Some mixed pseudobinary crystals exist over the whole concentration range,[1] such as isoelectronic $(Ca,Sr)F_2$, $(Ca,Ba)F_2$, and $(Ba,Sr)F_2$, or nonisoelectronic mixed systems, such as $(Cd,Pb)F_2$, $(Ca,Cd)F_2$, and $(Pb,Sr)F_2$.

Despite the availability of extensive experimental data,[2] the electronic-structure calculations, especially those based on first principles, for these compounds are still very few. Band-structure calculations for CaF_2 were performed by the tight-binding (TB) method[6] and by the orthogonalized-plane-wave[7] (OPW) and augmented-plane-wave (APW) methods. More recently, the band structures of CaF_2 and CdF_2 were determined[9] by the TB method for the valence states and by the pseudopotential method for the conduction bands. Self-consistent calculations by means of the linear combination of Gaussian orbitals (LCGO) method were performed[10] for CaF_2. In a recent paper,[11] the large-unit-cell complete neglect of differential overlap (LUC-CNDO) approximation in a quantum chemical scheme was applied to a number of the fluoride crystals, but only some band-structure characteristics (like the valence-band widths, the gaps, etc.) were given instead of more complete band-structure diagrams. Thus, no first-principles band structures of fluorite crystals were published until now for compounds other than CaF_2 and CdF_2. An important exception is

the band structure of PbF_2, deduced[12] from the results[9] for CdF_2 by means of Harrison's universal parametrization scheme[13] for solids. We note that from the experimental investigations[14] that one can expect the band structures of the crystals of SrF_2 and BaF_2 to be similar to that of CaF_2.

Even less is known about the electronic structure of mixed fluorite-type crystals, although it is clear from the optical studies of $(Cd,Pb)F_2$ that the dramatic irregularities in the spectroscopic behavior[4] must reflect some pronounced reconstruction of the electronic spectrum on the transition from CdF_2 to PbF_2. That this is really the case was demonstrated recently by Velický and Mašek, who performed[12] a parametrized tight-binding coherent-potential approximation (TB-CPA) study of the substitutional $(Cd,Pb)F_2$ random alloys, and obtained a reasonable agreement with photoemission experiments.[15] A similar dramatic reconstruction of the alloy electronic structure should be expected for other nonisoelectronic mixed crystals. On the other hand, the isoelectronic mixed crystals with ions coming from the IIa column of the Periodic Table [like, e.g., $(Ca,Sr)F_2$ mixed crystals] should not vary very much on alloying. LUC-CNDO supercell calculations simulating mixed crystals with a specific alloy composition were performed recently,[11] but the calculated characteristics do not allow a study of the concentration-induced changes observed in the photoemission experiments.

It is the main purpose of this paper to perform the comparative study of both pure and mixed fluoride crystals based on the first-principles linear-muffin-tin-orbital (LMTO) method[16] in the conjunction with the CPA to include the effect of the substitutional disorder. We shall employ to this end its tight-binding formulation[17] (TB-LMTO) generalized by us recently to random substitutional alloys (TB-LMTO-CPA method) with complex cubic lattice structures.[18] In some mixed crystals, of which the $(Cd,Pb)F_2$ alloy is the most striking example, large differences exist in the lattice constants of pure constituents[1] (about 10% for CdF_2 and PbF_2). Consequently, the problem of the bond-length variations in the random alloy is important, and we address it by considering two limiting situations: (i) one, in which the atomic structure is relaxed such that the nearest-neighbor distances preserve their values from the pure crystals, and (ii) another, where all interatomic distances, irrespective of the actual occupation of the lattice sites, scale linearly between the two pure-crystal limits. Both these cases can be simulated within the CPA calculations.

An alternative to the CPA is the supercell approach to the electronic structure of random alloys performed for a suitably chosen cluster of atoms, which is then repeated periodically. The standard band-structure techniques can then be applied within the supercell geometry[19] to obtain some electronic-structure characteristics, like the densities of states, alloy band gaps, etc. We discuss the applicability of the supercell approach in the alloy theory by comparing the LMTO calculations for the $Cd_2Pb_2E_4F_8$ supercell (E stands for empty spheres) and the TB-LMTO-CPA results for the $Cd_{0.5}Pb_{0.5}F_2$ random alloys, using the same potential parameters in both cases.

II. CALCULATION METHOD

The electronic structure of ordered crystals in the cubic fluorite structure was determined by the scalar-relativistic LMTO method in the atomic-sphere approximation (ASA) as described extensively in the literature.[16] Its tight-binding version, which is especially convenient when applied to random alloys,[18,20] was used for mixed crystals. The Hamiltonian of the pseudobinary $A_xB_{1-x}F_2$ (A,B = Ca,Sr,Cd,Pb) random alloys with the fluorite structure and in the orthogonal LMTO representation[17,18,20] reads

$$H_{RL,R'L'} = C_{RL}\delta_{RR'}\delta_{LL'} + \Delta_{RL}^{1/2}[S^0(1-\gamma S^0)^{-1}]_{RL,R'L'}\Delta_{R'L'}^{1/2} . \quad (1)$$

Here, R labels the site, and $L=(l,m)$ is the collective orbital-angular-momentum index. The interstitial empty spheres were included for a good space filling. Equal sphere sizes were used in order to minimize the overlap. With the abstraction of the atomic types, the underlying lattice is then bcc with a halved lattice constant, characterized by the canonical structure matrix S^0, which is nonrandom and independent of the lattice constant.[16] The fluorite structure is described as an interpretation of four fcc sublattices with the lattice constant a, shifted relative to each other by $(\frac{1}{4},\frac{1}{4},\frac{1}{4})a$. The first sublattice is occupied randomly by A and B atoms with probabilities x and $1-x$, respectively. The second and fourth sublattices are occupied by fluorines, and the third one by empty spheres. The scattering properties of atoms on sublattices are characterized by the potential parameters X_{RL} ($X=C,\Delta,\gamma$) entering the expression for the Hamiltonian. The potential parameters take two different values X_λ^Q ($Q=1,2$) on the sublattice σ, and $\lambda=(\sigma,L)$. The LMTO-ASA method within the local-density approximation (LDA) and the von Barth–Hedin parametrization for exchange and correlation was employed to generate the input potential parameters for the alloy calculations. The specific choices representing two different models of bond-length variations will be discussed in the next section. The reader interested in the details of the TB-LMTO-CPA method itself is referred to our recent papers, Refs. 18 and 20.

Concerning the application of the TB-LMTO-CPA method to the mixed fluoride crystals, two remarks are now in order. First, the energy gap is underestimated, as is usual within the LDA. An empirical correction can be made,[21] but here this was not attempted because we concentrate on the changes in the occupied states which appear to be sufficiently well described within the LDA. Further, reliable experimental data for the gaps at symmetry points are not available for most of the crystals studied. Second, it is commonplace in the LMTO-ASA method to use the sp^3d^5 partial waves at each atomic and empty site which leads, in the present case, to a 36×36 Hamiltonian matrix. The use of all orbitals is both unphysical and undesirable from interpretational and computational points of view. A minimal basis set consisting of only cation sd^5 states, the anion p^3 states, and the empty s states (13×13 model) gives an excellent descrip-

tion of occupied and low-lying conduction states, provided that the remaining states are not neglected, but are included approximately by means of Löwdin downfolding. The linearization of the contribution of the downfolded states is performed in a suitably chosen LMTO representation around the energy ε_0, which lies at the center of energy range of interest. This scheme allows us to determine the electronic structure of the random alloy from the minimal basis-set block of the fully averaged resolvent only, and thus simplify both the calculations and the physical interpretation of results. It is necessary to point out that for a description of valence states of a specific fluorite crystal, one can often use an even smaller minimal basis set, but for the application to random alloys this set must be common for both constituents. As concerns the principle of the linearized Löwdin downfolding, we refer the reader to Ref. 22, and, for its Green's-function reformulation suitable for the application to random alloys, to Ref. 18. We have demonstrated recently the efficiency of this approach in the case of the pseudobinary semiconductor alloy (Cd,Hg)Te with the zinc-blende structure[18] as well as for transition-metal disilicide pseudobinary (Co,Ni)Si_2 alloys with the fluorite structure.[23]

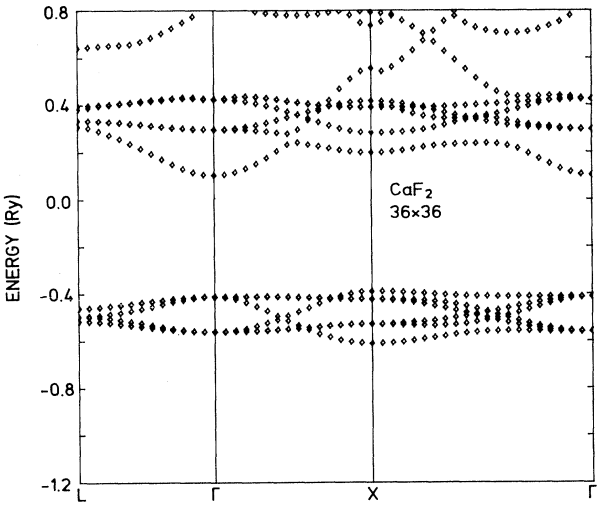

FIG. 1. Energy-band structure of CaF_2 along symmetry lines in the fcc Brillouin zone for the full 36×36 model.

III. RESULTS AND DISCUSSION

We shall discuss first the band structures of pure fluorides and relate their differences to the position of the cation in the Periodic Table. Then we examine the electronic structures of some mixed fluoride crystals. The concentration dependence of the densities of states and the Bloch spectral densities are presented, and special attention is devoted to the (Cd,Pb)F_2 system. Finally, we compare the results of the LMTO-CPA calculations with LMTO-supercell results for the $Cd_{0.5}Pb_{0.5}F_2$ mixed crystal. Emphasis is placed on the discussion of the valence states, while the conduction states will be mentioned only briefly. This problem will be addressed in detail in a future paper.

A. Band structures of pure fluorides

The energy-band structures of CaF_2, SrF_2, CdF_2, and PbF_2, determined by diagonalization of the Hamiltonian (1) in the full basis, are given in Figs. 1–4. The band structure of CaF_2 is the prototypical one for the whole family of fluorides. The valence bands are dominated by the F p states. On the contrary, the conduction bands are mostly formed by strongly mixed Ca s and Ca d states, and they are reminiscent in shape of the bands of metallic Ca. Our calculated CaF_2 bands agree well with those obtained by the LCGO method of Ref. 10. The band structure of SrF_2 is, with the exception of the narrower valence band, quite similar to that of CaF_2, as is expected (isoelectronic compound). Consequently, the alloying is not expected to cause dramatic changes in the mixed-crystal electronic structure. The case of CdF_2 is different. Contrary to the previous cases, the cation d states form a soft core lying close to the F p states. The upper part of the valence states originates from the F p orbitals with some admixture of the Cd d states. The lower part of the valence states is dominated by the Cd d states. The p-d hybridization in our calculations is more pronounced than in a combined tight-binding and pseudopotential method,[9] resulting in a different order of the energy bands. In this way, the valence-band shapes of CdF_2 differ in some details from the bands of CaF_2. This is in contrast to Refs. 6, 7, and 9, where the CdF_2 and CaF_2 bands are quite similar. We note that the bottom of the conduction states originates again from the Cd s states with some admixture of the F p states.

We have found no first-principles calculations for PbF_2

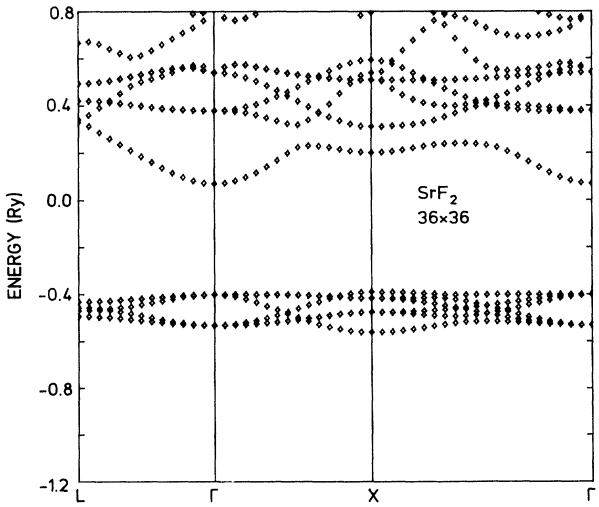

FIG. 2. As Fig. 1, but for SrF_2.

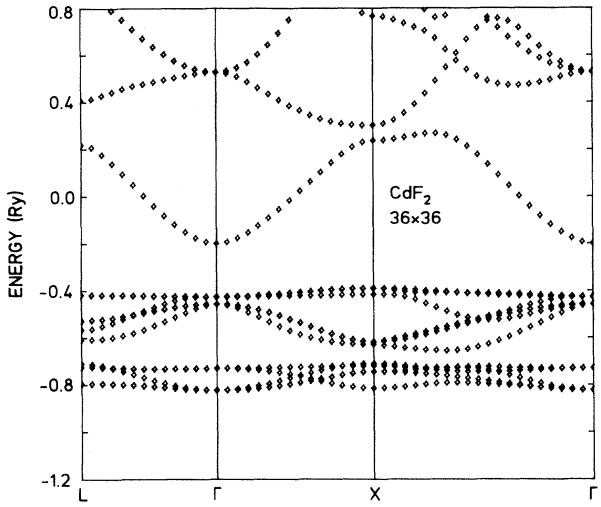

FIG. 3. As Fig. 1, but for CdF_2.

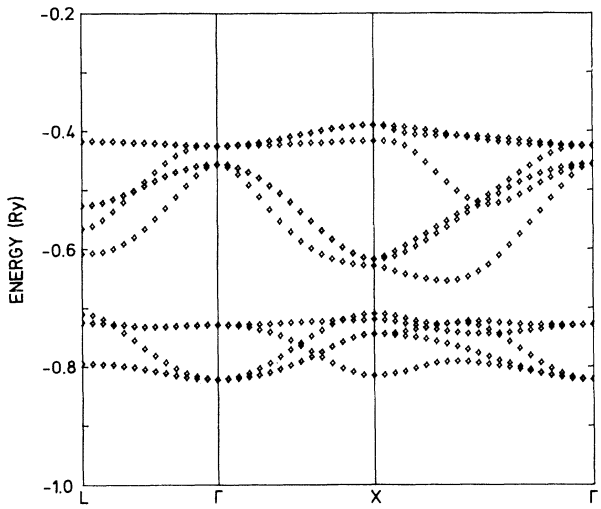

FIG. 5. Energy-band structure of CdF_2 along symmetry lines in the fcc Brillouin zone for the minimal-basis-set 13×13 model used in the alloy calculations. The energy of linearization of downfolded bands is $\varepsilon_0=-0.6$ Ry for the valence bands.

in the literature. The valence bands of PbF_2 differ significantly from those of CdF_2, because they originate from a strong hybridization between the F p and Pb s states. The latter ones contribute mostly to the lowest and the highest parts of valence bands. Another important feature of the band structure of PbF_2 is the "inverted" conduction band with the minima in the peripheral parts of the Brillouin zone. It is built mostly of the Pb p states. We note that the simple chemical picture used by Velický and Mašek and consisting[12] in a downward shift of cation s levels of CdF_2 gives a qualitatively correct description for both the valence and the lowest conduction bands in PbF_2. The Pb d states lie well outside the valence range. From the point of view of the alloy theory, we are thus faced with a complicated situation, where the cation s and d levels differ significantly in CdF_2 and PbF_2, indicating a so-called split-band limit regime. This automatically rules out the simplified treatments like the rigid-band model or the virtual-crystal approximation (VCA), but the case is well suited for the CPA method.[24] A similar dramatic reconstruction of the electron states is also expected in the other nonisoelectronic mixed crystals $(Ca,Cd)F_2$ and $(Pb,Sr)F_2$.

The minimal basis set $C(sd^5)F(p^3)E(s)F(p^3)$, where C stands for the cations, and with the energy of linearization chosen to be $\varepsilon_0=-0.6$ Ry, gives an excellent description of the occupied valence states for all studied fluoride crystals. As examples, Figs. 5 and 6 show the

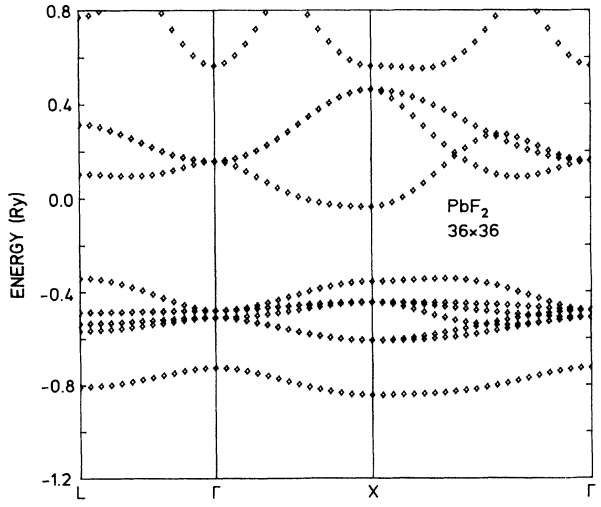

FIG. 4. As Fig. 1, but for PbF_2.

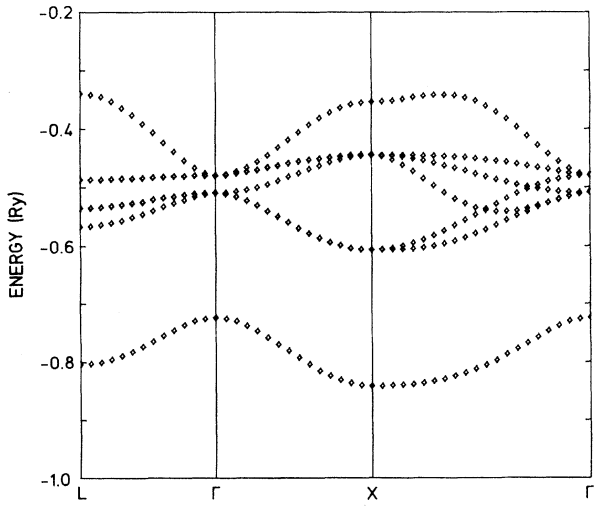

FIG. 6. As Fig. 3, but for PbF_2.

valence states of CdF_2 and PbF_2, over a reduced energy range. We note that even smaller minimal basis sets, $Cd(d^5)F(p^3)E(s)F(p^3)$ and $Pb(s)F(p^3)E(s)F(P^3)$, in particular cases, also give a very good description of the valence states. However, as mentioned in the preceding section, the minimal basis set must be common for both constituents when applied to disordered alloys within the CPA.[18] A different minimal basis set could be chosen for a proper description of well-separated conduction states, but this problem is not addressed here.

B. Properties of pseudobinary mixed crystals

The concentration dependence of the total densities of states (DOS's) for the $(Ca,Sr)F_2$ mixed crystal is presented in Fig. 7. This alloy exhibits only a weak off-diagonal or bandwidth disorder, connected primarily with the different lattice constants of CaF_2 and SrF_2 [$a(CaF_2)=5.462$ Å and $a(SrF_2)=5.796$ Å]. The calculations were done using the minimal basis set $C(sd^5)F(p^3)E(s)F(p^3)$, with $C=$Ca,Sr (13×13 model). The two-peak form characteristic for both pure CaF_2 and SrF_2 crystals is preserved, and the effect of alloying consists in the increase of the alloy valence-band width (consisting of F p states) with Ca concentration.

The Bloch spectral densities for the $Ca_{0.5}Sr_{0.5}F_2$ system are plotted in Fig. 8. In crystals, the Bloch spectral densities consist of δ-function peaks situated at energies $E_\nu(\mathbf{k})$, where ν is the band index. For weak disorder, they have Lorentzian shapes and are centered around the virtual-crystal energies, corresponding to common alloy bands. In strongly disordered alloys, these peaks are shifted and broadened by the disorder. It is seen that the lower part of the spectra (for $E<-0.45$ Ry) is influenced by the disorder more than the upper part. However, the sharpness of the spectral density peaks (see, for example, $k=k_\Gamma$) indicates that the effect of disorder in this alloy system is rather weak.

The corresponding results for $(Ca,Cd)F_2$ and $(Pb,Sr)F_2$ mixed crystals are presented in Figs. 9–11. The lattice mismatch is rather small in both cases. The calculations were done with the same minimal basis set as before. The total DOS's for CaF_2 and SrF_2 have already been discussed. It is thus instructive to characterize briefly the

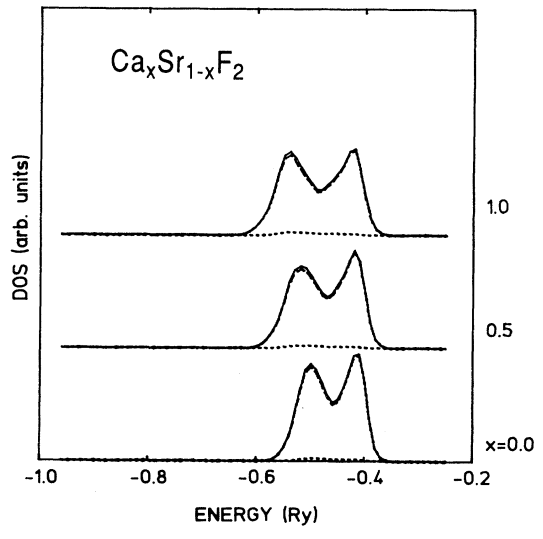

FIG. 7. The total density of states for $Ca_xSr_{1-x}F_2$ pseudobinary mixed crystals (solid lines) and their decomposition into the minimal-basis-set (dashed lines) parts and the contribution of the remaining downfolded states (dotted lines). The concentrations x are assigned to the corresponding curves (13×13 model, $\varepsilon_0=-0.6$ Ry).

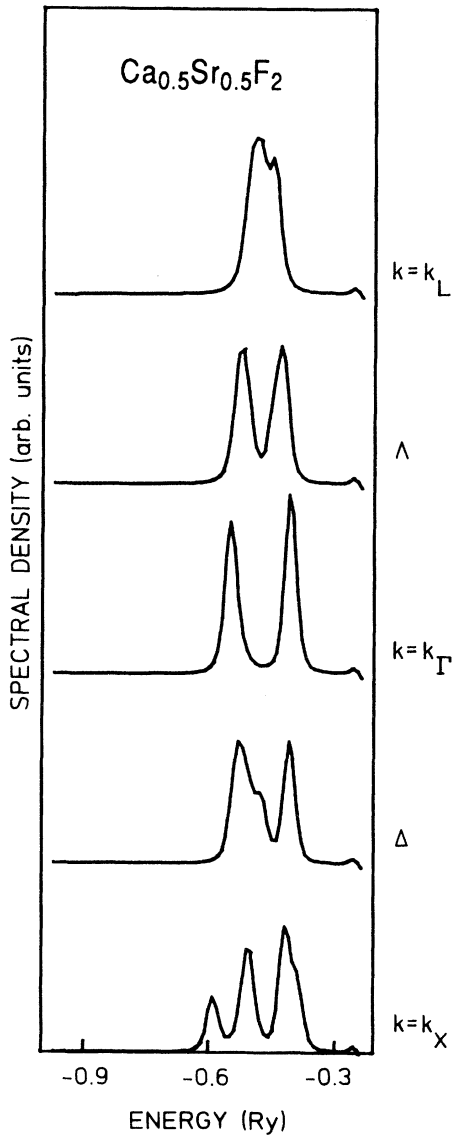

FIG. 8. The Bloch spectral densities for the $Ca_{0.5}Sr_{0.5}F_2$ mixed crystal along the symmetry line $L-X$ in the fcc Brillouin zone.

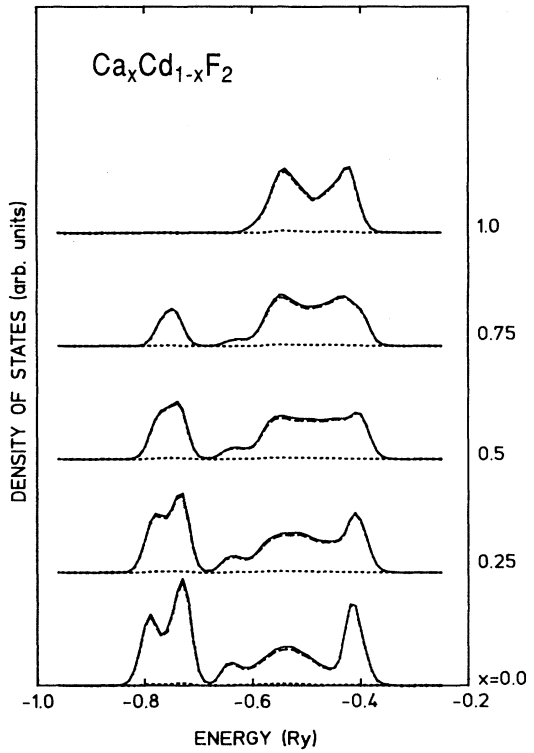

FIG. 9. As Fig. 7, but for $Ca_xCd_{1-x}F_2$ mixed crystals.

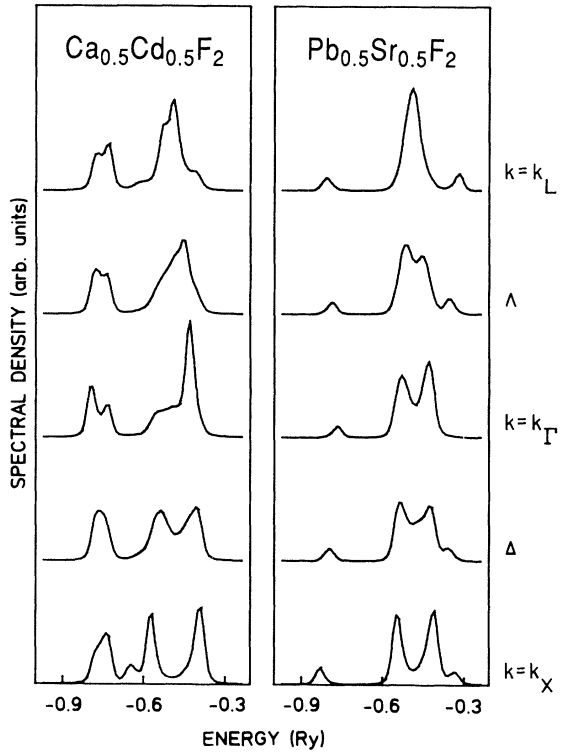

FIG. 11. The same as in Fig. 8, but for $Ca_{0.5}Cd_{0.5}F_2$ (left frame) and $Pb_{0.5}Sr_{0.5}F_2$ (right frame) mixed crystals.

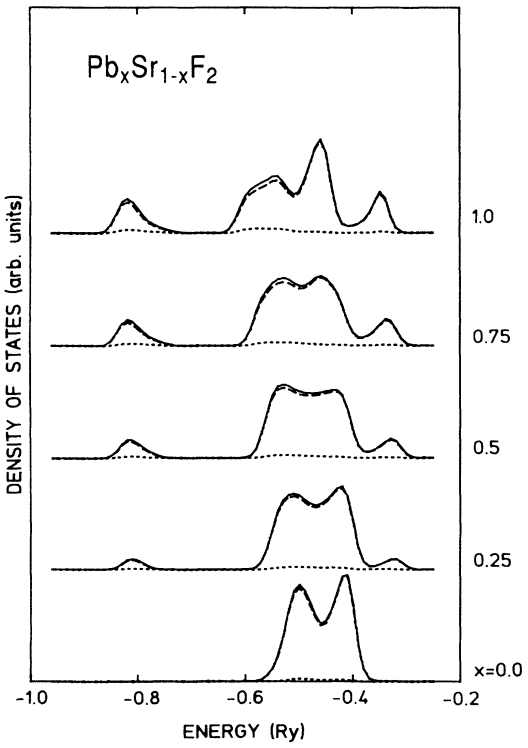

FIG. 10. As Fig. 7, but for $Pb_xSr_{1-x}F_2$ mixed crystals.

changes in the total DOS functions induced by Cd and Pb impurities in CaF_2 and SrF_2 crystals, respectively. The DOS's of pure CdF_2 and PbF_2 crystals will be discussed in connection with the analysis below of $(Cd,Pb)F_2$ mixed crystals. The most pronounced feature of the concentration dependence of the total DOS for the $(Ca,Cd)F_2$ system is the development of the Cd d-related features in the lower part of the alloy band. A similar effect at the low and high ends of the alloy valence band in $(Pb,Sr)F_2$ mixed crystals is due to the Pb s states. We also note the concentration-induced shape changes of the dominating F p band complex is in both cases more pronounced for $(Ca,Cd)F_2$, which is due to the strong hybridization of the F p states with the cation Cd d states.

The corresponding Bloch spectral densities for both equiconcentration mixed crystals are shown in Fig. 11. The k-dispersive peaks for E between -0.6 and -0.4 Ry belong to common weakly perturbed F p bands, while nearly nondispersive peaks at $E \approx -0.75$ Ry are due to Cd d states, and the only slightly k-dependent peaks at $E \approx -0.8$ and -0.35 Ry are due to Pb s states.

We shall now discuss in detail the results for the most interesting mixed-crystal case, $(Cd,Pb)F_2$. The additional complication connected with the presence of the disorder in this system is the large lattice constant mismatch[1] of CdF_2 and PbF_2 [$a(CdF_2)=5.388$ Å and $a(PbF_2)=5.941$ Å]. This, in turn, should introduce pronounced bond-length variations in the random alloys, as is well known

from $A^{III}B^{V}$ and $A^{II}B^{IV}$ pseudobinary semiconductor alloys,[25,26] deduced in both cases from the extended x-ray-absorption fine-structure spectroscopy (EXAFS) measurements. According to these measurements, the bond lengths AC and BC in pseudobinary alloys $A_xB_{1-x}C$ remain essentially independent of the concentration x, and have the same values as in the pure crystals. Because no similar measurements exist for this system, and in order to investigate the effect of bond-length variations on the electronic structure, we have evaluated the electronic structure of $Cd_xPb_{1-x}F_2$ random alloys in two extreme limits: model A, where the nearest-neighbor distances in alloys are the same as those in pure crystals, and are independent of the alloy composition; model B, where the nearest-neighbor distances are all the same, and scale linearly with composition between the values for CdF_2 and PbF_2.

Model A is realized in the TB-LMTO-CPA as follows. The variations of the bond lengths are transformed into the variations of the corresponding hopping matrix elements. Neglecting any angle distortions due to the nonequal bond lengths, the structure matrix S^0 is the same for all compositions. Only the potential parameters should be evaluated for Wigner-Seitz radii, which are different for different cations in the mixed crystal. Assuming simply that the atomic volume in the alloy is, for both components, the same as in pure crystals, we use as an input the self-consistent-potential parameters obtained from the LMTO method for CdF_2 and PbF_2 at their (different) equilibrium lattice constants. Because the atomic and empty spheres fill all the space, Vegard's law for alloys is satisfied statistically, on the average. It is important to note that the potential parameters of fluorine are different in CdF_2 and PbF_2 due to different chemical environments (Cd or Pb), but the dominant effect is due to different lattice constants of CdF_2 and PbF_2 (the p-band width potential parameter Δ_p of F in CdF_2 is about 50% larger than that of F in PbF_2). To account for this, we average in some way the CdF_2 and PbF_2 potential parameters on F sites. For example, one can average them in proportion to the number of neighboring Cd and Pb atoms to the F atom. Here, we have averaged these differences within the CPA. We note that the TB-LMTO-CPA treats the diagonal as well as off-diagonal randomness in the Hamiltonian (1) on the same footing.[20]

In the other limit, model B, we use as an input the LMTO potential parameters determined for the supercells with the formula $Cd_nPb_{4-n}E_4F_8$, and with the Wigner-Seitz radii being the same for all sites and varying linearly with the concentration x. Then, the bond-length distances for a given composition are all the same, and Vegard's law is satisfied explicitly. With $n=0-4$, this would simulate alloys $Cd_xPb_{1-x}F_2$ with $x=0.25n$. A similar approach, based on the mixed-basis pseudopotential method, was used recently[19] to determine the band-structure characteristics of some $A^{II}B^{VI}$ pseudobinary semiconductor alloys. Here we do something less restrictive: the supercell calculations are only used to generate reliable potential parameters to be employed later on in the CPA calculations. The potential parameters for $CdF_2(PbF_2)$ crystals and $Cd_4E_4F_8$ ($Pb_4E_8F_8$) supercells differ only negligibly, which guarantees the internal consistency of this approach. We note, for completeness, that model A was implicitly used in previous mixed crystals (Figs. 7–11). The differences between the lattice constants of the pure compounds, which form the mixed crystals, were much smaller in those cases than for $(Cd,Pb)F_2$. Consequently, the differences between models A and B also become smaller.

The concentration dependence of the total DOS for $(Cd,Pb)F_2$ alloys within model A is presented in Fig. 12. The upper part of the valence states of CdF_2 has a three-peak structure dominated by F p states, while the lower part of the spectra consists of Cd d states, which exhibit a two-peak form. All this is observed in recent photoemission spectra (PES) measurements, although[15] it should be kept in mind that the direct comparison of the total DOS and PES is not fully justified.[27] The PbF_2 valence states consist predominantly of F p states hybridized with Pb s states. The lowest and highest valence peaks show a strong admixture of the Pb s states. The most pronounced effect of alloying is a strong depletion of the Cd d-related features with increasing Pb content. This is clearly reflected in the PES experiment.[15] Another feature is a narrowing of the dominating F-related part of the spectra when going from CdF_2 to PbF_2, which is also observed experimentally. Also, we note the increase of the Pb-related features at the top and bottom of the spec-

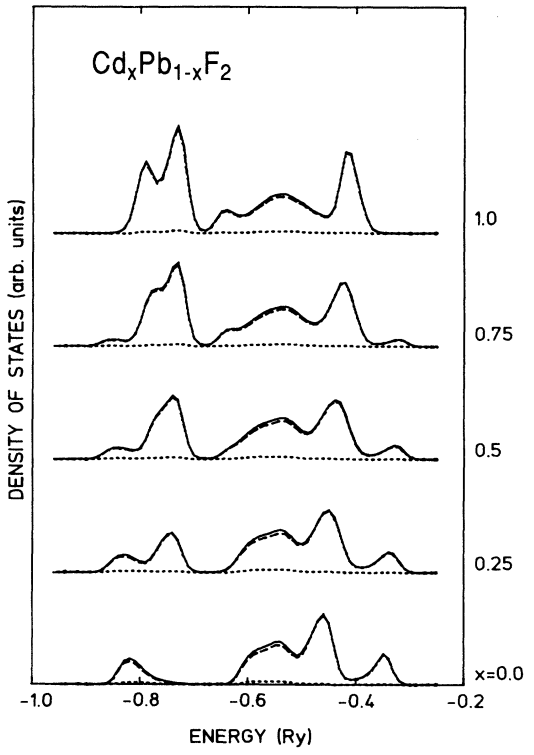

FIG. 12. As Fig. 7, but for $Cd_xPb_{1-x}F_2$ mixed crystals (model A).

tra with increasing Pb concentration. The latter feature is also found in the simplified TB-CPA theory of Ref. 12, but the former effects are missing due to the lack of the cation d states in the basis set and the concentration dependence of the fluorine TB parameters. The calculations further show that the states treated approximately by means of downfolding contribute very little to the total DOS. This justifies our choice of the minimal basis set.

The decomposition of the total DOS for the $Cd_{0.5}Pb_{0.5}F_2$ alloy within model A into various parts is presented in Fig. 13. The lowest and highest peaks in the spectra are dominated by the Pb s states, the Cd d contribution being limited to the lower part of the alloy valence band. The split-band character of the strong d scattering is clearly seen on comparing the Cd d and Pb d parts: the Pb d states lie well outside the alloy valence band. The split-band behavior is also seen, to a certain extent, for the Cd s and Pb s states.

The concentration dependence of the total DOS for the $(Cd,Pb)F_2$ alloy within model B is given in Fig. 14. The results are similar, the most pronounced qualitative difference being the concentration development of the Pb s-induced states above the common fluorine band. While the distance of the dominating fluorine peak around -0.45 Ry and the Pb s-induced peak slightly decreases with decreasing Pb content in model A, in quali-

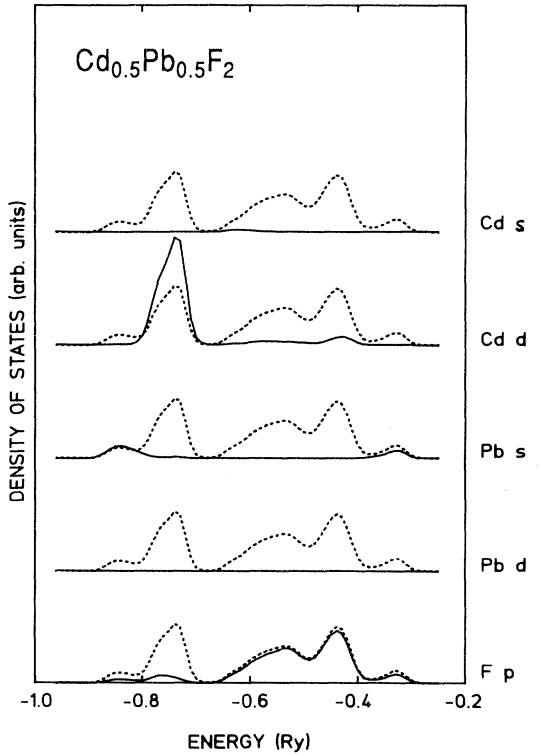

FIG. 13. The decomposition of the total density of states corresponding to the minimal basis set for $Cd_{0.5}Pb_{0.5}F_2$ mixed crystal (dotted lines) in model A into Cd s, Cd d, Pb s, Pb d, and F p contributions (not concentration weighted).

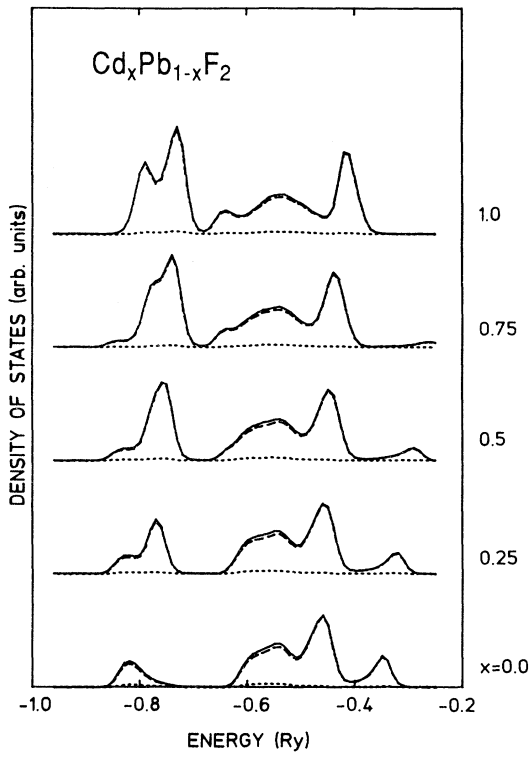

FIG. 14. As Fig. 7, but for $Cd_xPb_{1-x}F_2$ mixed crystals (model B).

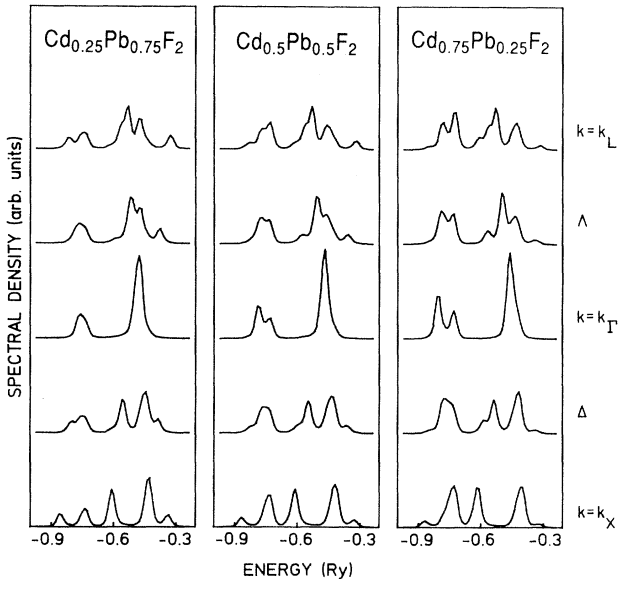

FIG. 15. As Fig. 8, but for $Cd_{0.25}Pb_{0.75}F_2$ (left frame), $Cd_{0.5}Pb_{0.5}F_2$ (middle frame), and $Cd_{0.75}Pb_{0.25}F_2$ (right frame) mixed crystals.

tative agreement with the experiment,[15] the same distance increases in model *B*. This suggests that the model assuming the preservation of bond lengths from the pure constituents, supported by EXAFS experiments on the pseudobinary semiconductor alloys with the zinc-blende structure, and indicated by the x-ray photoemission spectroscopy (XPS) measurements on the $(Cd,Mn)F_2$ system,[5] could also be valid for the mixed $(Cd,Pb)F_2$ crystals.

The Bloch spectral densities for $Cd_xPb_{1-x}F_2$ random alloys with $x=0.25$, 0.5, and 0.75 are shown in Fig. 15. Let us discuss in some detail the Cd-rich and Pb-rich cases. The lower part of the spectra for the Cd-rich alloy along the $L-\Gamma$ line is dominated by two, nearly nondispersive, Cd *d* peaks. These peaks are broadened by the disorder in the Pb-rich alloy, and they survive resolved only close to the *L* point. Note, however, that the positions of these peaks are nearly concentration independent. In contrast, the VCA would predict strong concentration-dependent positions of common Cd and Pb *d* bands. Clearly, the VCA fails in this strong-scattering regime. Another interesting feature is the Cd-induced peak near -0.75 Ry at the *X* point in the Pb-rich alloy. No states are present in this energy range in the pure PbF_2. Similarly, although less pronounced, are the Pb-derived peaks below (above) a common fluorine band complex for $E\approx -0.85$ $(E\approx -0.35)$ Ry at $k=k_X(k=k_L)$ for the Cd-rich alloy. The remaining k-dispersive peaks in the energy range -0.65 to -0.4 Ry correspond to common, weakly perturbed F *p* bands.

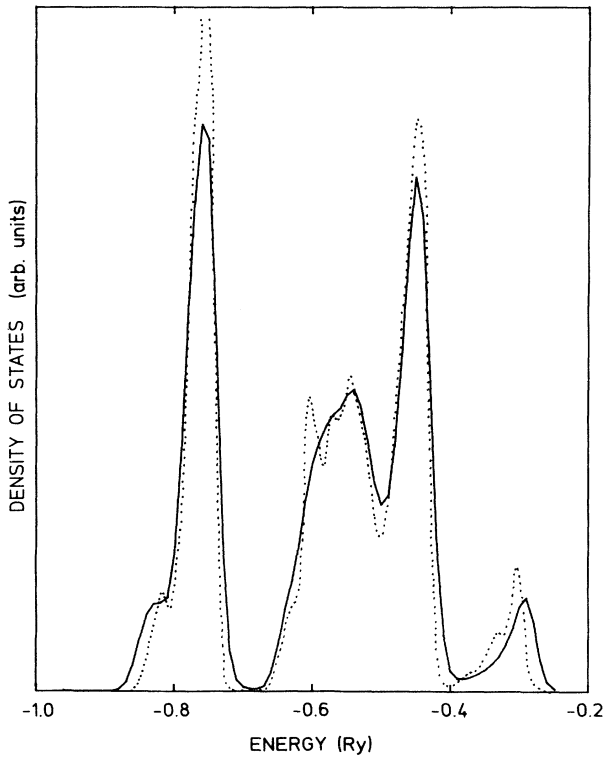

FIG. 16. The total density of states for the $Cd_{0.5}Pb_{0.5}F_2$ mixed crystal (solid line, 13×13 model, ε_0-0.6 Ry) and for the $Cd_2Pb_2E_4F$ supercell (dotted line) using the same (supercell) potential parameters.

C. Comparison of the LMTO-CPA and LMTO-supercell methods

We now address the question of the applicability of the supercell approach to random alloys. The answer depends sensitively on the physical quantity of interest and, of course, on the system considered. The supercell method is certainly less convenient[28] for obtaining such subtle details of the electronic structure as the damping of various bands and related problems, because it still assumes the perfect periodicity in the arrangement of supercells. On the other hand, gross features like the total energy or the density of states should be described reasonably well by the supercell method because the scattering problem on atoms within a supercell (e.g., the *d* scattering on Cd and Pb atoms in the $Cd_2Pb_2E_4F_8$ supercell) is represented properly, in contrast to the VCA approach. In Fig. 16 we compare the total DOS's obtained from the CPA calculations for the $Cd_{0.5}Pb_{0.5}F_2$ mixed crystal with the corresponding results for the $Cd_2Pb_2E_4F_8$ supercell, using the same (supercell) potential parameters in both cases (model *B*). Apart from the broadening in the CPA-DOS, the agreement between the two curves is very good. Note a slight upward shift of the Pb *s*-related peak at -0.3 Ry in the CPA-DOS as compared with the supercell DOS. This indicates one of the future improvements to be made on existing theories, namely, the determination of the input parameters for the CPA calculations from the supercell method for a suitably chosen supercell with internally relaxed atomic positions to account for possible bond-length variations. The TB-LMTO-CPA method seems to be especially suitable for such a project.

IV. CONCLUSION

We have presented an *ab initio* study of the electronic structure of random pseudobinary mixed crystals with the fluorite-type structure, using the TB-LMTO-CPA approach combined with the empty-sphere concept for a good space filling, and with Löwdin downfolding to take full advantage of the minimal basis set. We have found that the minimal basis set consisting of the cation sd^5 orbitals, fluorine p^3 orbitals, and *s* orbitals at the interstitial empty spheres, gives an excellent description of the valence bands of calcium, strontium, cadmium, and lead fluorides and their mixed crystals. The electronic structures of $(Cd,Pb)F_2$, $(Ca,Cd)F_2$, and $(Pb,Sr)F_2$ mixed crystals exhibit a dramatic reconstruction during the concentration development, which is due to very different hybridization of the fluorine *p* states with the cation *s* and *d* states in the valence energy range of constituent crystals. This, in turn, is a result of very different positions of cation *s* and *d* levels in the pure crystals, indicating a strong-level disorder, which must be treated properly. For constituent cations from the same column of the Periodic Table (Ca and Sr), the effect of disorder is weak-

er than in the former alloys, where the constituent cations come from the different columns. The results for $(Cd,Pb)F_2$ alloys agree reasonably well with the available experimental data, indicating that the model assuming approximate preservation of the pure-constituent bond lengths in mixed fluoride crystals is more justified than the model assuming the same bond lengths among atoms varying linearly with the alloy composition. It would be interesting to verify this conclusion by performing the EXAFS measurements on $(Cd,Pb)F_2$ mixed crystals. As a side issue, we have verified that the supercell approach based on the 16-site supercell gives, for the total DOS, results which agree reasonably well with those obtained from the CPA for the same potential parameters.

*Permanent address: Institute of Physics, Czechoslovak Academy of Sciences, Na Slovance 2, 180 40 Praha, Czechoslovakia.

[1]W. Pies and A. Weiss, in *Crystal Structure of Inorganic Compounds: Key Elements F,Cl,Br,I*, edited by K. -H. Hellwege and A. M. Hellwege, Landolt-Börnstein, New Series, Vol. III/7a (Springer, Berlin 1973).

[2]See Refs. 6 and 7 for the list of relevant experimental papers.

[3]J. M. Réau, P. P. Fedorov, L. Rabardel, S. F. Matar, and P. Hagenmuller, Mater. Res. Bull. **18**, 1235 (1983).

[4]I. Kosacki and J. M. Langer, Phys. Rev. B **33**, 6 (1986).

[5]B. J. Kowalski, V. Cháb, and B. A. Orlowski, Phys. Rev. B **36**, 7642 (1987).

[6]N. V. Starostin and V. A. Ganin, Fiz. Tverd. Tela (Leningrad) **15**, 3404 (1973) [Sov. Phys.—Solid State **15**, 2265 (1974)].

[7]N. V. Starostin and M. P. Shepilov, Fiz. Tverd. Tela (Leningrad) **17**, 882 (1975) [Sov. Phys.—Solid State **17**, 523 (1975)].

[8]V. V. Nemoshkalenko, V. C. Aleshin, and M. T. Panchenko, Dokl. Akad. Nauk SSSR **231**, 585 (1976).

[9]J. P. Albert, C. Jouanin, and C. Gout, Phys. Rev. B **16**, 4619 (1977).

[10]R. A. Heaton and C. C. Lin, Phys. Rev. B **22**, 3629 (1980).

[11]R. A. Evarestov, I. V. Murin, and A. V. Petrov, J. Phys. Condens. Matter **1**, 6603 (1989).

[12]B. Velický and J. Mašek, Solid State Commun. **58**, 663 (1986).

[13]W. A. Harrison, *Electronic Structure and the Properties of Solids* (Freeman, San Francisco, 1980).

[14]R. T. Pole, R. C. Leckey, and J. Liesegang, Phys. Rev. B **12**, 5872 (1975).

[15]V. Cháb, B. Kowalski, and B. A. Orlowski, Solid State Commun. **58**, 667 (1986).

[16]O. K. Andersen, Phys. Rev. B **12**, 3060 (1975); H. L. Skriver, *The LMTO Method* (Springer, Heidelberg, 1983).

[17]O. K. Andersen and O. Jepsen, Phys. Rev. Lett. **53**, 2571 (1984).

[18]J. Kudrnovský, V. Drchal, M. Šob, N. E. Christensen, and O. K. Andersen, Phys. Rev. B **40**, 10 029 (1989).

[19]J. E. Bernard and A. Zunger, Phys. Rev. B **36**, 3199 (1987).

[20]J. Kudrnovský, V. Drchal, and J. Mašek, Phys. Rev. B **35**, 2487 (1987); J. Kudrnovský and V. Drchal, *ibid.* **41**, 7515 (1990).

[21]N. E. Christensen, Phys. Rev. B **30**, 5753 (1984).

[22]W. R. L. Lambrecht and O. K. Andersen, Phys. Rev. B **34**, 2439 (1986).

[23]J. Kudrnovský and N. E. Christensen, Solid State Commun. (to be published).

[24]Alternatively, one can use either the recursion method applied to a cluster of atoms [L. C. Davis, Phys. Rev. B **28**, 6961 (1983)], or the standard band-structure technique within the supercell method, Ref. 19, and later in this section.

[25]J. C. Mikkelsen, Jr. and J. B. Boyce, Phys. Rev. B **28**, 7130 (1983)

[26]W.-F. Pong, R. A. Mayanovic, and B. A. Bunker, Physica B **158**, 617 (1989).

[27]The matrix-element effects can modify the strength of various peaks, depending on the frequency of exciting source. The comparison with the results of Ref. 15 is further complicated by the uncertainty of the wave-vector determination during the experiment, so that the spectra are probably partly angle integrated.

[28]The noticeable exception is the evaluation of the concentration dependence of a gap in pseudobinary $A^{III}B^{V}$ or $A^{II}B^{VI}$ semiconductor alloys (see, e.g., Ref. 19), because the states around the gap at Γ are only weakly damped, as contrasted with the deep-lying valence states.